

## Article

# Study of the Structure, Magnetic, Thermal and Electrical Characterisation of $\text{ZnCr}_2\text{Se}_4$ : Ta Single Crystals Obtained by Chemical Vapour Transport

Izabela Jendrzewska <sup>1,\*</sup>, Tadeusz Gron <sup>2</sup>, Piotr Kwapuliński <sup>3</sup>, Joachim Kusz <sup>2</sup>, Ewa Pietrasik <sup>1</sup>, Tomasz Goryczka <sup>3</sup>, Bogdan Sawicki <sup>2</sup>, Andrzej Ślebarski <sup>2</sup> , Marcin Fijałkowski <sup>2</sup>, Josef Jampilek <sup>4</sup>  and Henryk Duda <sup>2</sup>

<sup>1</sup> Institute of Chemistry, University of Silesia in Katowice, 40-007 Katowice, Poland; ewa.pietrasik@us.edu.pl

<sup>2</sup> Institute of Physics, University of Silesia in Katowice, 40-007 Katowice, Poland; tadeusz.gron@us.edu.pl (T.G.); joachim.kusz@us.edu.pl (J.K.); bogdan.sawicki@us.edu.pl (B.S.); andrzej.slebarski@us.edu.pl (A.Ś.); marcin.fijalkowski@us.edu.pl (M.F.); henryk.duda@us.edu.pl (H.D.)

<sup>3</sup> Institute of Materials Science, University of Silesia in Katowice, 40-007 Katowice, Poland; piotr.kwapulinski@us.edu.pl (P.K.); tomasz.goryczka@us.edu.pl (T.G.)

<sup>4</sup> Department of Analytical Chemistry, Faculty of Natural Sciences, Comenius University, 842 15 Bratislava, Slovakia; josef.jampilek@gmail.com

\* Correspondence: izabela.jendrzewska@us.edu.pl



**Citation:** Jendrzewska, I.; Gron, T.; Kwapuliński, P.; Kusz, J.; Pietrasik, E.; Goryczka, T.; Sawicki, B.; Ślebarski, A.; Fijałkowski, M.; Jampilek, J.; et al. Study of the Structure, Magnetic, Thermal and Electrical Characterisation of  $\text{ZnCr}_2\text{Se}_4$ : Ta Single Crystals Obtained by Chemical Vapour Transport. *Materials* **2021**, *14*, 2749. <https://doi.org/10.3390/ma14112749>

Academic Editor: Christian Müller

Received: 23 April 2021

Accepted: 20 May 2021

Published: 22 May 2021

**Publisher's Note:** MDPI stays neutral with regard to jurisdictional claims in published maps and institutional affiliations.



**Copyright:** © 2021 by the authors. Licensee MDPI, Basel, Switzerland. This article is an open access article distributed under the terms and conditions of the Creative Commons Attribution (CC BY) license (<https://creativecommons.org/licenses/by/4.0/>).

**Abstract:** The new series of single-crystalline chromium selenides, Ta-doped  $\text{ZnCr}_2\text{Se}_4$ , was synthesised by a chemical vapour transport method to determine the impact of a dopant on the structural and thermodynamic properties of the parent compound. We present comprehensive investigations of structural, electrical transport, magnetic, and specific heat properties. It was expected that a partial replacement of Cr ions by a more significant Ta one would lead to a change in direct magnetic interactions between Cr magnetic moments and result in a change in the magnetic ground state and electric transport properties of the  $\text{ZnCr}_{2-x}\text{Ta}_x\text{Se}_4$  ( $x = 0.05, 0.06, 0.07, 0.08, 0.1, 0.12$ ) system. We found that all the elements of the cubic system had a cubic spinel structure; however, the doping gain linearly increased the  $\text{ZnCr}_{2-x}\text{Ta}_x\text{Se}_4$  unit cell volume. Doping with tantalum did not significantly change the semiconductor and magnetic properties of  $\text{ZnCr}_2\text{Se}_4$ . For all studied samples ( $0 \leq x \leq 0.12$ ), an antiferromagnetic order (AFM) below  $T_N \sim 22$  K was observed. However, a small amount of Ta significantly reduced the second critical field ( $H_{c2}$ ) from 65 kOe for  $x = 0.0$  ( $\text{ZnCr}_2\text{Se}_4$  matrix) up to 42.2 kOe for  $x = 0.12$ , above which the spin helical system changed to ferromagnetic (FM). The  $H_{c2}$  reduction can lead to strong competition among AFM and FM interactions and spin frustration, as the specific heat under magnetic fields  $H < H_{c2}$  shows a strong field decrease in  $T_N$ .

**Keywords:** single crystals; semiconductors; antiferromagnetic; specific heat

## 1. Introduction

Single crystals are required in many fields of modern technology and the electronic industry. They are used for lasers, as an optical component for spectroscopy, in oscillators, in light-emitting diodes and in innumerable other devices. Among seleno-spinel crystals such as  $\text{AB}_2\text{Se}_4$  matrices, where A and B are the metallic ions occupying tetra- and octahedral sites, respectively, and matrices diluted with non-magnetic ions, due to the large cubic unit cell (about  $10 \text{ \AA}$ ), the effects of site disorder, lattice frustration and random distribution of spin interactions [1–5] create new potential applications.

The  $\text{ZnCr}_2\text{Se}_4$  belongs to the group of seleno-spinels and crystallises in a cubic system (SG:  $Fd\bar{3}m$ , No. 27),  $a = 10.4891 \text{ \AA}$  [6]. This compound is a  $p$ -type semiconductor with a helical magnetic structure. Magnetic interactions are the result of the existence of exchangeable Cr–Cr interactions competing with each other. The Cr–Se–Cr interaction causes the ferromagnetic (FM) ordering of the magnetic moments of chromium ions. In contrast, the

Cr–Se–Se–Cr and Cr–Se–Zn–Se–Cr interactions lead to antiferromagnetic (AFM) ordering. The FM interactions are evidenced by the positive value of paramagnetic Curie–Weiss temperature  $\theta_{CW} = 115$  K and AFM interactions are present below  $T_N \approx 21$  K [7–10]. An increasing dc magnetic field shifts  $T_N$  to lower temperatures during a susceptibility peak in the paramagnetic region—to higher ones. Next, the first critical field  $H_{c1}$  values connected with a metamagnetic transition decrease slightly with temperature. The values of the second critical field,  $H_{c2}$ , connected with the breakdown of the conical spin structure, drop rapidly with temperature, suggesting a spin frustration of the re-entrant type [2]. Low-angle neutron scattering (SANS) measurements showed the absence of any long-range magnetic order in the high-field (spin-nematic) phase, as well as the fact that all observed phase transitions were surprisingly isotropic concerning the field direction [11].

The introduction of the third cation to the  $\text{ZnCr}_2\text{Se}_4$  crystal lattice, depending on many factors, may have a strong influence on changes in physicochemical properties. The most important factors are: (a) the size of the ion radius, (b) the position of the ion in the spinel structure (tetra- or octahedral), (c) the coordination number (CN), (d) the type of chemical bond [12]. Substitution of an additional cation into the  $\text{ZnCr}_2\text{Se}_4$  matrix resulted in such phenomena as the appearance of spin glass [13–15], polaron conductivity [16], ferrimagnetism [17] and the enhancement of both FM [18,19] and AFM interactions [20,21].

This article describes the family of  $\text{ZnCr}_2\text{Se}_4$  single crystals, doped with Ta, obtained by chemical vapour transport (CVT method), as well as their physicochemical properties. The purpose of the present study was to investigate the effect of the Ta ion admixture on the stability of the cubic symmetry and the physical (magnetic, electrical, thermal) properties of a  $\text{ZnCr}_2\text{Se}_4$ -based spinel. This work continues our previous works focusing on modifying  $\text{ZnCr}_2\text{Se}_4$  properties by incorporating the additional *d*-electronic elements into the crystal lattice. In this study, we used a computer simulation of the mechanism of chemical vapour transport. To the best of our knowledge, this is the first demonstration of the synthesis of  $\text{ZnCr}_2\text{Se}_4$  single crystals containing tantalum ions and their properties.

## 2. Materials and Methods

Commercially available high-purity elements Zn, Ta, Cr, Se (5N, Sigma Aldrich, Poznań, Poland) and anhydrous  $\text{CrCl}_3$  (Sigma Aldrich, Poznań, Poland) were used in the present study. Synthesis of  $\text{ZnCr}_2\text{Se}_4$ : Ta single crystals was carried out using a chemical transport reaction method. Chemical vapour transport is a method in which a solid substance is transferred using the reversible gaseous reaction from the  $T_1$  temperature (dissolution zone) to the  $T_2$  temperature (crystallisation zone). The partial equilibrium pressures of the components  $p_i$  depend on the value of the equilibrium constant  $K_a$  of the reaction, which can occur at a given temperature. The most significant changes in  $p_i$  occur when  $K_a$  reaches a value close to 1 ( $\log K_a \approx 0$ ).

For this purpose, a thermodynamic model of  $\text{ZnCr}_2\text{Se}_4$ : Ta single-crystal growth was prepared. To determine the ability and conditions of transport reaction, a set of all the hypothetical reactions that may appear in the  $\text{ZnSe}$ -Ta-Se- $\text{CrCl}_3$  system was created. These reactions, which were used to determine the dependence of  $\log K_a$  values on the temperature, were calculated using the HSC Chemistry computer programme (HSC Chemistry ver. 6.01, Release 2009, Metso Outotec Corporation, Helsinki, Finland) [22]. In this case, the modified chemical vapour transport method was used. The single crystals of  $\text{ZnCr}_2\text{Se}_4$ : Ta were grown from the binary selenide ZnSe, pure Ta and Se, and with  $\text{CrCl}_3$  as a transport carrier. Therefore, the hypothetical reaction set included the reactions of binary ZnSe, pure tantalum and selenium with  $\text{CrCl}_3$  and the dissociation products of  $\text{CrCl}_3$  ( $\text{CrCl}_4$  and  $\text{Cl}_2$ ). The ZnSe was obtained by the ceramic method [14,18]. Mixtures of the ZnSe, Ta, Se and  $\text{CrCl}_3$  were placed in quartz ampoules (length—200 mm, inner diameter—20 mm) evacuated to  $10^{-5}$  mbarr. The ampoules were placed in a two-zone tubular furnace. The furnace was cooled for 24 h, after around 500 h of heating. The chemical composition of the obtained single crystals and their surfaces were studied by scanning electron microscopy (SEM) Jeol 6480 (JEOL USA, INC., Peabody, MA, USA), with a propertied energy-dispersive

X-ray spectrometer (SEM/EDS). Four single crystals with differing tantalum content were chosen for X-ray diffraction (XRD) measurements (Table 1). The structural parameters were determined using a SuperNova X-ray diffractometer (Agilent, Oxfordshire, UK). The technical details and the computer programmes used are described in [21,23].

**Table 1.** Conditions of growth and chemical composition of  $\text{ZnCr}_2\text{Se}_4$ : Ta single crystals.  $T_d$  is the temperature of the dissolution zone,  $T_c$  is the temperature of the crystallisation zone and  $\Delta T$  is the difference in temperature between the dissolution and the crystallisation zones.

No.	Nominal Formula	$T_d$ (K)	$T_c$ (K)	$\Delta T$ (K)	% Weight				Real Chemical Formula
					Zn	Cr	Ta	Se	
(1)	$\text{Zn}_{0.9}\text{Ho}_{0.1}\text{Cr}_2\text{Se}_4$	1223	1153	70	$13.29 \pm 0.09$	$20.66 \pm 0.06$	$1.99 \pm 0.01$	$64.06 \pm 0.04$	$\text{Zn}_{1.05}\text{Cr}_{1.95}\text{Ta}_{0.05}\text{Se}_4$
(2)	$\text{Zn}_{0.9}\text{Ho}_{0.1}\text{Cr}_2\text{Se}_4$	1133	1083	50	$13.22 \pm 0.08$	$20.53 \pm 0.07$	$2.14 \pm 0.02$	$64.11 \pm 0.05$	$\text{Zn}_{0.99}\text{Cr}_{1.94}\text{Ta}_{0.06}\text{Se}_4$
(3)	$\text{Zn}_{0.8}\text{Ho}_{0.2}\text{Cr}_2\text{Se}_4$	1203	1143	60	$13.08 \pm 0.06$	$20.37 \pm 0.06$	$2.45 \pm 0.05$	$64.10 \pm 0.03$	$\text{Zn}_{0.99}\text{Cr}_{1.93}\text{Ta}_{0.07}\text{Se}_4$
(4)	$\text{Zn}_{0.8}\text{Ho}_{0.2}\text{Cr}_2\text{Se}_4$	1203	1153	50	$13.12 \pm 0.02$	$20.12 \pm 0.04$	$2.68 \pm 0.06$	$64.18 \pm 0.03$	$\text{Zn}_{0.99}\text{Cr}_{1.82}\text{Ta}_{0.08}\text{Se}_4$
(5)	$\text{Zn}_{0.7}\text{Ho}_{0.3}\text{Cr}_2\text{Se}_4$	1203	1133	70	$13.13 \pm 0.03$	$19.75 \pm 0.05$	$3.25 \pm 0.03$	$63.87 \pm 0.03$	$\text{Zn}_{0.99}\text{Cr}_{1.89}\text{Ta}_{0.10}\text{Se}_4$
(6)	$\text{Zn}_{0.7}\text{Ho}_{0.3}\text{Cr}_2\text{Se}_4$	1203	1143	60	$13.21 \pm 0.02$	$19.53 \pm 0.04$	$3.92 \pm 0.04$	$63.34 \pm 0.02$	$\text{Zn}_{1.00}\text{Cr}_{1.87}\text{Ta}_{0.12}\text{Se}_4$

The electrical resistivity  $\rho(T)$  was measured by the four-point DC method with an accuracy of around  $\pm 0.6\%$  using a KEITHLEY 6517B Electrometer/High Resistance Meter (Keithley Instruments, LLC, Solon, OH, USA) in the temperature range of 77–400 K. A Quantum Design SQUID-based MPMSXL-5-type magnetometer (Quantum Design, San Diego, CA, USA) to determine the specific heat and magnetic parameters in the temperature range 10–300 K was used. Measurements were carried out at a magnetic field of 100 Oe for both in the ZFC (zero-field cooling) and FC (field cooling) mode. The Néel temperature and the critical fields were determined as the temperature corresponding to  $d\chi/dT$  vs.  $T$  and  $dM/dH$  vs.  $H$ . The effective magnetic moment was determined using the following equation [24,25]:

$$\mu_{eff} = \sqrt{\frac{3k_B C}{N_A \mu_B^2}} \cong 2.828\sqrt{C} \quad (1)$$

where  $k_B$  is the Boltzmann constant,  $N_A$  is the Avogadro number,  $\mu_B$  is the Bohr magneton, and  $C$  is the molar Curie constant. The magnetic superexchange integrals for the first two coordination spheres  $J_1$  and  $J_2$  were calculated using the Holland and Brown equations [26].

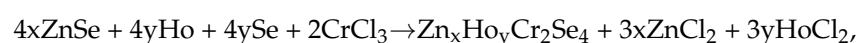
$$T_N = -5J_1 + 10J_2, \theta = 15J_1 + 90J_2 \quad (2)$$

The methods used to determine the electrical properties and specific heat are described in detail in [17,18,20]. Thermogravimetry and differential scanning calorimetry (TG/DSC) were carried out using a Labsys Evo system, with a heating rate of 5 °C/min and in an inert gas atmosphere (Ar).

### 3. Results and Discussion

#### 3.1. Growth of Single Crystals and Chemical Composition

Synthesis of the single crystals of  $\text{ZnCr}_2\text{Se}_4$ : Sn was carried out according to the reaction:



where:  $y = 0.1, 0.2, 0.3$  and  $x = 1 - y$ .

We synthesised the samples with an amount of Ta ions higher than 0.3. For the samples with  $y = 0.4, 0.5$ , we did not observe single crystals in ampoules. One of the main reasons is that one end member of the  $\text{Zn}_x\text{Ta}_y\text{Cr}_2\text{Se}_4$  series, i.e.,  $\text{TaCr}_2\text{Se}_4$ , does not exist. Based on the reactions presented in Figure 1, it can be assumed that volatile zinc and selenium compounds are formed in the ZnSe-Ta-Se- $\text{CrCl}_3$  system, e.g.,  $\text{ZnCl}_2$ ,  $\text{Zn}_2\text{Cl}_4$ ,  $\text{SeCl}_2$ ,  $\text{SeCl}_4$  and  $\text{Se}_2$ . Thermodynamic calculations showed that in the ZnSe-Ta-Se- $\text{CrCl}_3$  system, ZnSe

and Se are mainly transported by gaseous  $\text{CrCl}_3$  and  $\text{CrCl}_4$  (values of  $\log K_a$  are close to zero in the selected temperature range: 1000–1400 K; Figures 1 and 2).

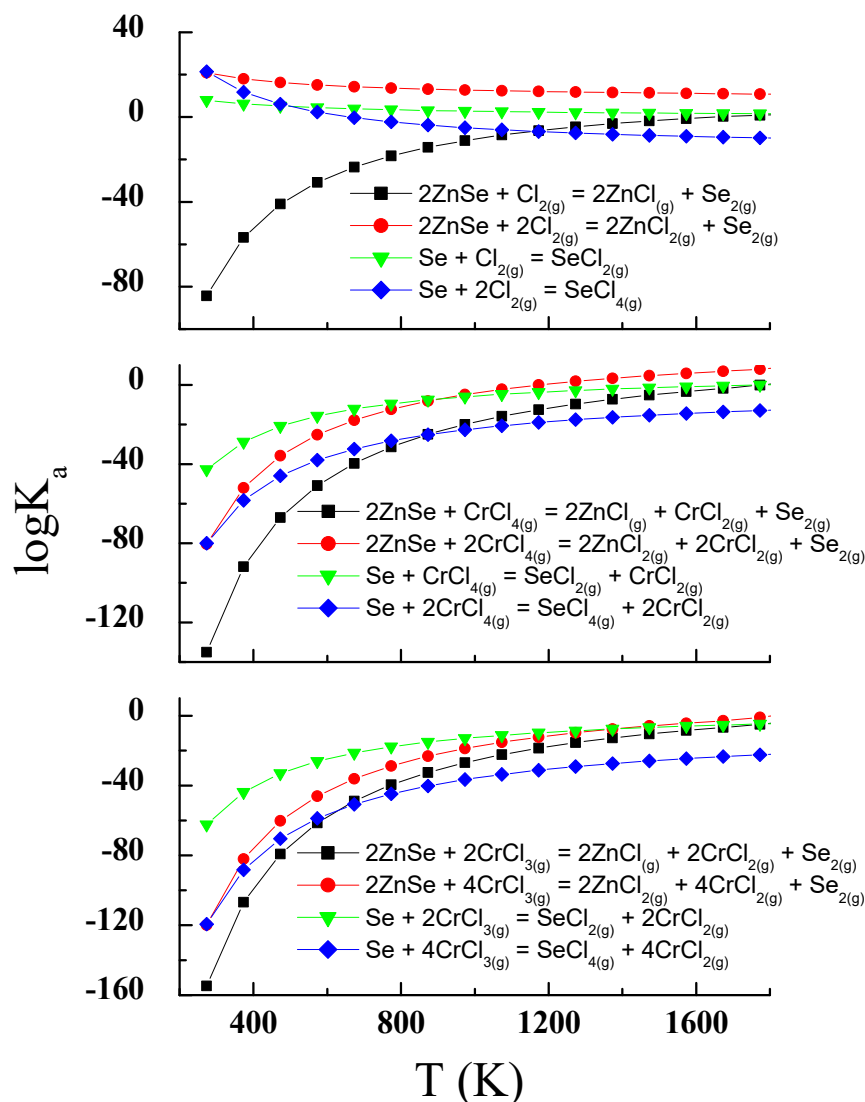


**Figure 1.** The dependence of the  $\log K_a$  vs. temperature  $T$  for the ZnSe and pure Se transporting reactions.

The transport reactions presented in Figure 2 show that volatile tantalum compounds can be formed in the ZnSe-Ta-Se- $\text{CrCl}_3$  system, e.g.,  $\text{TaCl}$ ,  $\text{TaCl}_2$ ,  $\text{TaCl}_3$ ,  $\text{TaCl}_4$  and  $\text{TaCl}_5$ . For  $\text{CrCl}_4$ ,  $\log K_a$  reaches values close to zero at lower temperatures than for  $\text{CrCl}_3$ . It can therefore be assumed that the chemical transport for Ta occurs mainly with  $\text{CrCl}_4$ . The  $\log K_a$  of the transport reactions with  $\text{CrCl}_3$  and  $\text{CrCl}_4$  for tantalum has values and shapes similar to the corresponding Zn and Se transport reactions (Figure 1). Thus, the conditions for the simultaneous transport of ZnSe, Ta and Se, and spinel crystallisation, are met. Calculated  $\log K_a$  values for transport reactions with chlorine are close to zero at higher temperatures. This indicates that chlorine is not involved in the transport process in the selected temperature range. Based on these calculations, the reaction conditions were chosen (temperatures of the dissolution and crystallisation zones and their difference). The crystallisation zone temperature was between 1070 and 1180 K. The melting zone temperature was in the range 1175–1233 K. Their difference was 50–70 K. Smaller differences in temperature ( $\Delta T$ ) are more favourable for the crystallisation process. The choice of reaction conditions was based on our experience with the growth of  $\text{ZnCr}_2\text{Se}_4$  single crystals. The best results have been achieved using temperatures of the dissolution zone

in the range 1123–1223 K. The choice of the reaction temperature is also limited by the thermal endurance of silica glass (~1500 K). These reaction conditions allowed us to obtain single crystals of good quality (Figure 3).

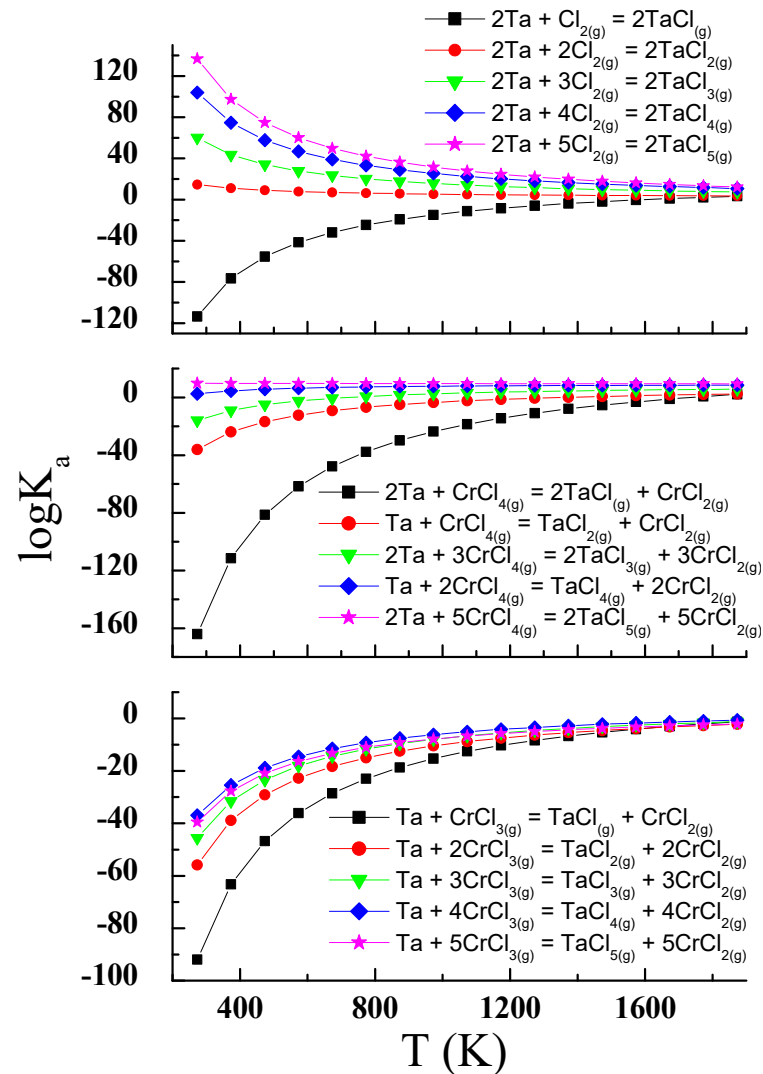


Figure 2. The dependence of the  $\log K_a$  vs. temperature  $T$  for the pure Ta transporting reactions.

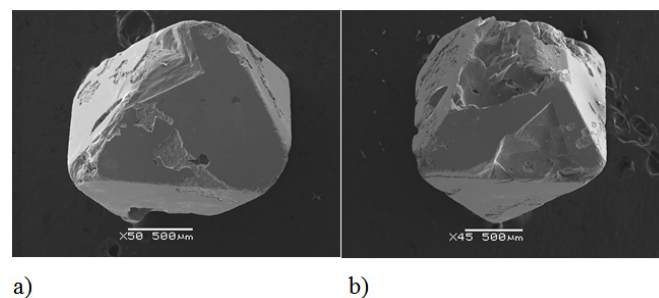


Figure 3. Examples of single crystals obtained in the  $\text{ZnCr}_2\text{Se}_4$ : Ta system: (a)  $\text{Zn}_{1.03}\text{Cr}_{1.96}\text{Ta}_{0.05}\text{Se}_4$ , (b)  $\text{Zn}_{0.99}\text{Cr}_{1.89}\text{Ta}_{0.10}\text{Se}_4$ .

To determine the average chemical composition, measurements were carried out at 20 different locations of the single crystal. Each of the measuring areas was approximately  $50 \times 30 \mu\text{m}$ . Then, the average chemical composition was calculated. The error bar

represents standard deviation. Relatively low values of standard deviation indicate good homogeneity of the chemical composition. Details of the reaction conditions and results of SEM measurements are presented in Table 1.

As shown in Table 1, the determined real chemical composition showed a lower amount of incorporated tantalum than the nominal composition. On the one hand, this may be due to the lower amount of tantalum transported to the crystallisation zone. On the other hand, the separation of tantalum from the system during the dissolution and crystallisation processes is likely.

### 3.2. Structural Study

The origin of the unit cell is agreed with the point  $\bar{3}m$  of the space group  $Fd\bar{3}m$  (No. 227). In a normal spinel, the  $Zn^{2+}$  ions occupy the tetrahedral position 8a:  $1/8, 1/8, 1/8$  (A site), and the  $Cr^{3+}$  ions occupy the position 16d:  $\frac{1}{2}, \frac{1}{2}, \frac{1}{2}$  (B site). To determine the cation distribution, two models were taken into account for each composition.

The first model of the structure refinement was considering the Ta ions' presence in the A sites (tetrahedral) with coupled site occupancy factors (SOF) and constrained atomic displacements. Due to the strong correlation, the SOFs for Zn and Ta were refined separately in alternative calculations. The convergence caused the rejection of Ta ions from the tetrahedral sites.

The same procedure was applied to Ta ions occupied by the B sites (octahedral). This approach led to acceptable atomic displacement parameters and SOFs, which allowed for description of the general chemical formula for obtained single crystals as presented in Tables 2 and 3. On the other hand, a slightly increased thermal shift at the B site may indicate a static disturbance in the position of the  $Cr^{3+}/Ta^{3+}$  pseudoion, which is mainly caused by the difference in ionic charges and in ionic and covalent radii ( $r_i(Zn^{2+}) = 0.60 \text{ \AA}$ ,  $r_i(Cr^{3+}) = 0.62 \text{ \AA}$ ,  $r_i(Ta^{3+}) = 0.72 \text{ \AA}$  and  $R_c(Zn^{2+}) = 0.74 \text{ \AA}$ ,  $R_c(Cr^{3+}) = 0.76 \text{ \AA}$ ,  $R_c(Ta^{3+}) = 0.86 \text{ \AA}$ , respectively) [27]. Based on the structural study, the formula describing cation distribution in the system is:  $ZnCr_{2-x}Ta_xSe_4$ , where  $x = 0.05, 0.06, 0.07, 0.08, 0.10$  and  $0.12$ , which is shown in Tables 2 and 3. In these chemical compositions, the region of the solubility limit of tantalum in the  $ZnCr_{2-x}Ta_xSe_4$  system was found to be equal to  $0.12$ . The structural study showed the obtained  $ZnCr_{2-x}Ta_xSe_4$  single crystals crystallise in a cubic system with space group  $Fd\bar{3}m$  (No.227,  $Z = 8$ ). The lattice parameters of the obtained single crystals were larger than the lattice parameter of non-substituted  $ZnCr_2Se_4$  ( $a = 10.489 \text{ \AA}$ ) and increased with the rising amount of tantalum (Table 2).

**Table 2.** Structural parameters of the  $ZnCr_{2-x}Ta_xSe_4$  single crystals.

Chemical Formula	Lattice Parameter (Å)	Volume (Å <sup>3</sup> )	Density Calc. (Mg/m <sup>3</sup> )	Absorption Coeff. (mm <sup>-1</sup> )	Goodness of Fit on F <sup>2</sup>	R Parameters	
						R <sub>1</sub>	wR <sub>2</sub>
ZnCr <sub>1.95</sub> Ta <sub>0.05</sub> Se <sub>4</sub>	10.4786(12)	1150.56(4)	5.679	33.717	1.128	0.0122	0.0335
ZnCr <sub>1.94</sub> Ta <sub>0.06</sub> Se <sub>4</sub>	10.4794(3)	1150.82(2)	5.693	33.801	1.123	0.0145	0.0423
ZnCr <sub>1.93</sub> Ta <sub>0.07</sub> Se <sub>4</sub>	10.4832(9)	1152.08(9)	5.701	33.827	1.156	0.0195	0.0500
ZnCr <sub>1.92</sub> Ta <sub>0.08</sub> Se <sub>4</sub>	10.4938(12)	1155.56(2)	5.700	33.834	1.156	0.0179	0.0534
ZnCr <sub>1.90</sub> Ta <sub>0.10</sub> Se <sub>4</sub>	10.5003(15)	1157.73(3)	5.712	33.852	1.213	0.0155	0.0451
ZnCr <sub>1.88</sub> Ta <sub>0.12</sub> Se <sub>4</sub>	10.5069(18)	1159.90(3)	5.737	33.880	1.234	0.0164	0.0423

Tantalum ions accommodated the octahedral sites, substituting  $Cr^{3+}$  ions. The enhancement of the lattice parameters was linear (Figure 4) and confirmed the presence of tantalum ions as  $Ta^{3+}$  in the crystal lattice of  $ZnCr_2Se_4$ . This phenomenon is consistent with the differences between the ionic radii of  $Zn^{2+}$ ,  $Ta^{3+}$  (in octahedral coordination) and  $Cr^{3+}$ . The positional parameter of Se ( $u$ ), which is a measure of the anion sublattice distortion from the cubic close packing, did not change significantly from the ideal value of  $x = 0.250$ . The tantalum amount did not influence the  $u$  parameter. The slight differences between the tested single crystals were in the range of the standard deviation (Table 3). The same was observed in the metal–metal and metal–selenium distances (Table 4), where the differences

were insignificant. The structure refinement parameters are presented in Table 3, while the selected bond distances and angles are shown in Table 4.

**Table 3.** Atomic coordinates and equivalent isotropic displacement parameters of the  $\text{ZnCr}_{2-x}\text{Ta}_x\text{Se}_4$  ( $x = 0.05, 0.06, 0.07, 0.08, 0.10$  and  $0.12$ ) single crystals. The Wyckoff positions of the atoms in the spinel structure are: Zn in  $8b$  ( $3/8, 3/8, 3/8$ ); Cr/Ta in  $16c$  ( $\frac{1}{2}, \frac{1}{2}, \frac{1}{2}$ ) and Se in  $32e$  ( $x, x, x$ ).

Spinel	Anion Parameter $u$	SOF in A Site		SOF in B Site		$U_{\text{iso}}$ ( $\text{\AA} \times 10^3$ )		
		Zn	Cr/Ta	Zn	Cr/Ta	Cr/Ta	Se	
$\text{ZnCr}_{1.95}\text{Ta}_{0.05}\text{Se}_4$	0.2594(1)	1.0	1.951:0.049(9)	8.73(15)	5.77(15)	6.13(12)		
$\text{ZnCr}_{1.96}\text{Ta}_{0.04}\text{Se}_4$	0.2594(1)	1.0	1.961:0.039(9)	8.83(15)	5.65(15)	6.24(12)		
$\text{ZnCr}_{1.93}\text{Ta}_{0.07}\text{Se}_4$	0.2594(1)	1.0	1.929:0.071(9)	8.83(15)	5.65(15)	6.24(12)		
$\text{ZnCr}_{1.92}\text{Ta}_{0.08}\text{Se}_4$	0.2594(2)	1.0	1.919:0.081(1)	8.24(18)	7.14(17)	7.57(12)		
$\text{ZnCr}_{1.90}\text{Ta}_{0.10}\text{Se}_4$	0.2594(2)	1.0	1.902:0.098(2)	8.80(17)	6.15(16)	6.27(12)		
$\text{ZnCr}_{1.88}\text{Ta}_{0.12}\text{Se}_4$	0.2594(1)	1.0	1.879:0.121(3)	8.67(12)	5.98(14)	6.54(12)		

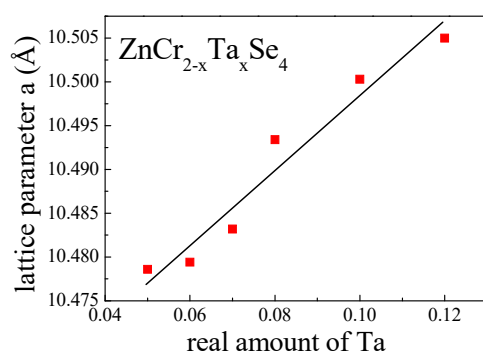


**Figure 4.** Dependence of the lattice parameters of  $\text{ZnCr}_{2-x}\text{Ta}_x\text{Se}_4$  single crystals on the amount of tantalum.

**Table 4.** Selected interatomic distances ( $\text{\AA}$ ) and bond angles (deg) of the  $\text{ZnCr}_{2-x}\text{Ta}_x\text{Se}_4$  spinel single crystals.

Spinel	Bond Distances		Bond Angles	
	Zn-Se	Cr/Ta-Se	Se-Zn-Se	Se-Cr/Ta-Se
$\text{ZnCr}_{1.95}\text{Ta}_{0.05}\text{Se}_4$	2.4388(3)	2.5252(2)	$109.5(0) \times 6$	$180.0(0) \times 3$ $94.543(7) \times 6$ $85.457(9) \times 6$
$\text{ZnCr}_{1.94}\text{Ta}_{0.06}\text{Se}_4$	2.4401(3)	2.5248(2)	$109.5(0) \times 6$	$180.0(0) \times 3$ $94.574(7) \times 6$ $85.4426(9) \times 6$
$\text{ZnCr}_{1.93}\text{Ta}_{0.07}\text{Se}_4$	2.4407(4)	2.5253(2)	$109.5(0) \times 6$	$180.0(0) \times 3$ $94.575(9) \times 6$ $85.425(9) \times 6$
$\text{ZnCr}_{1.92}\text{Ta}_{0.08}\text{Se}_4$	2.4450(4)	2.5299(2)	$109.5(0) \times 6$	$180.0(0) \times 3$ $94.575(8) \times 6$ $82.425(8) \times 6$
$\text{ZnCr}_{1.90}\text{Ta}_{0.10}\text{Se}_4$	2.4454(4)	2.55137(2)	$109.5(0) \times 6$	$180.0(0) \times 3$ $94.555(8) \times 6$ $85.445(8) \times 6$
$\text{ZnCr}_{1.88}\text{Ta}_{0.12}\text{Se}_4$	2.4482(4)	2.55543(2)	$109.5(0) \times 6$	$180.0(0) \times 3$ $94.575(8) \times 6$ $85.425(8) \times 6$

### 3.3. Electrical and Magnetic Properties

The electrical measurements of  $\text{ZnCr}_{2-x}\text{Ta}_x\text{Se}_4$  ( $x = 0.5, 0.6, 0.7, 0.8, 0.10$  and  $0.12$ ) showed the semiconducting properties and thermally activated conduction in the intrinsic region (200–400 K) with the activation energy of  $E_a \sim 0.22$  eV. In the extrinsic region (77–125 K), the activation of electrical conductivity was not observed (Figure 5). The influence of anisotropy on the value of electrical resistivity in the studied spinel single crystals was not observed, as in the  $\text{CuCr}_{1.6}\text{V}_{0.4}\text{Se}_4$  spinel single crystal, in which the resistance was measured in the direction of [001] and [111] [28].

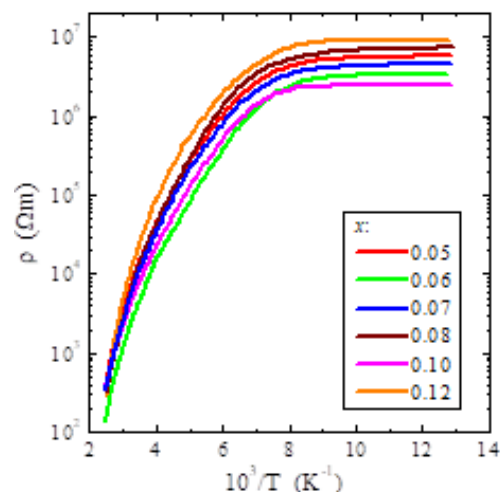


**Figure 5.** Electrical resistivity ( $\ln\rho$ ) vs. reciprocal temperature  $10^3/T$  of  $\text{ZnCr}_{2-x}\text{Ta}_x\text{Se}_4$  single crystals (where  $x = 0.05, 0.06, 0.07, 0.08, 0.10$  and  $0.12$ ).

A similar dependence of electrical resistance  $\rho(T)$  on temperature was observed by Watanabe [29] in  $\text{ZnCr}_2\text{Se}_4$  single crystals measured in different crystallographic directions. No significant influence of the crystallographic orientation on the value of the specific electrical resistance was observed. This may have been because the spinel structure had a high cubic symmetry. The SANS measurements also confirmed the isotropic phase transitions with respect to the field direction in the monocrystalline  $\text{ZnCr}_2\text{Se}_4$  spinel [11]. The observed  $\rho(T)$  dependence in Figure 5 means that doping of the  $\text{ZnCr}_2\text{Se}_4$  single crystals under study with tantalum did not affect the thermal activation of electrical conductivity.

The results of magnetic measurements of  $\text{ZnCr}_{2-x}\text{Ta}_x\text{Se}_4$  spinels are shown in Figures 6–8 and Table 5. The dependence of the dc (in both ZFC and FC mode) showed an AFM order below the Néel temperature  $T_N \sim 22$  K and FM short-range interactions, evidenced by the positive Curie–Weiss temperature  $\theta_{CW} < 100$  K. The  $T_N$  temperature essentially does not depend on the concentration of Ta ion. On the other hand, these ions strongly influence the short-range magnetic interactions visible for different values of  $\theta_{CW}$  (Table 5).

The results mentioned above were confirmed by the negative values of the superexchange integral for the first coordination sphere ( $J_1$ ) and the positive values of the superexchange integral for the second coordination sphere ( $J_2$ ) (Table 5). The effective magnetic moment calculated from the magnetic susceptibility expansion at high temperature corresponded to the effective number of Bohr magnetons estimated for the corresponding content of  $x$  chromium ions, as the tantalum ion was in the +III oxidation state of the octahedral site in the spinel structure. However, an additional magnetic ion may appear when tantalum is in the +II or +IV oxidation state. Then, its magnetic susceptibility is in the order of  $154 \times 10^{-6}$  emu/mol at 293 K. No split of the ZFC–FC susceptibility was observed, which suggests a lack of spin frustration in the studied single crystals (Figure 6).

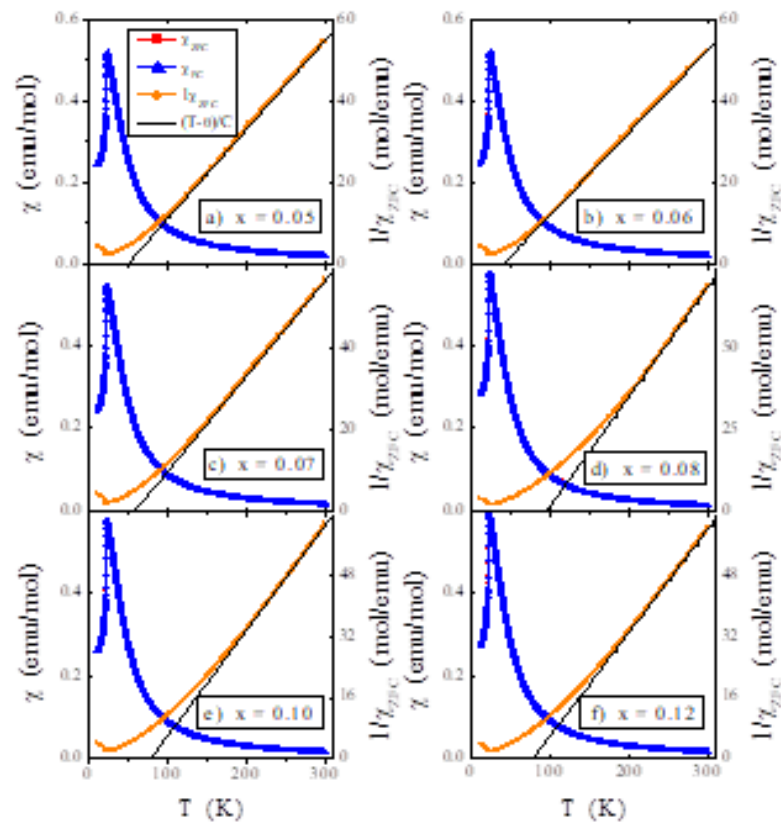


**Figure 6.** ZFC and FC magnetic susceptibility  $\chi$  vs. temperature  $T$  of  $\text{ZnCr}_{2-x}\text{Ta}_x\text{Se}_4$  single crystals, where (a) 0.05, (b) 0.06, (c) 0.07, (d) 0.08, (e) 0.10 and (f) 0.12 recorded at  $H = 100$  Oe. The solid (black) line,  $(T - \theta)/C$ , indicates Curie–Weiss behaviour.

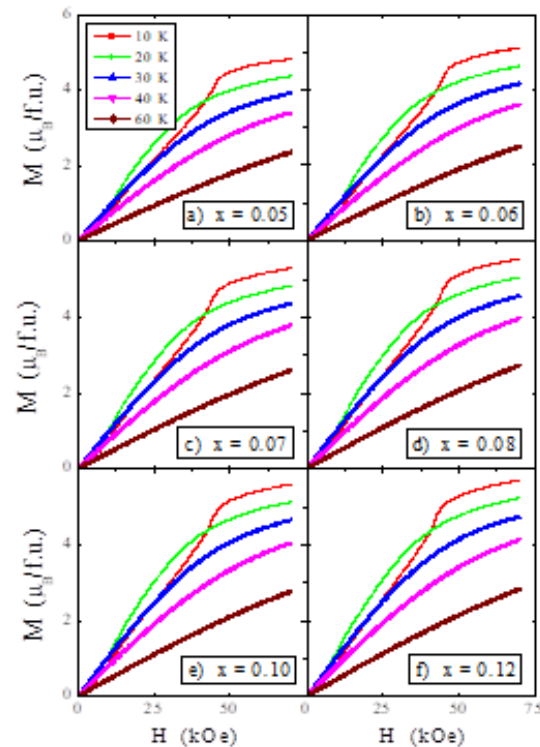


**Figure 7.** Magnetisation  $M$  vs. temperature  $T$  of  $\text{ZnCr}_{2-x}\text{Ta}_x\text{Se}_4$  single crystals, where (a) 0.05, (b) 0.06, (c) 0.07, (d) 0.08, (e) 0.10 and (f) 0.12 recorded at 10, 20, 30, 40 and 60 K.

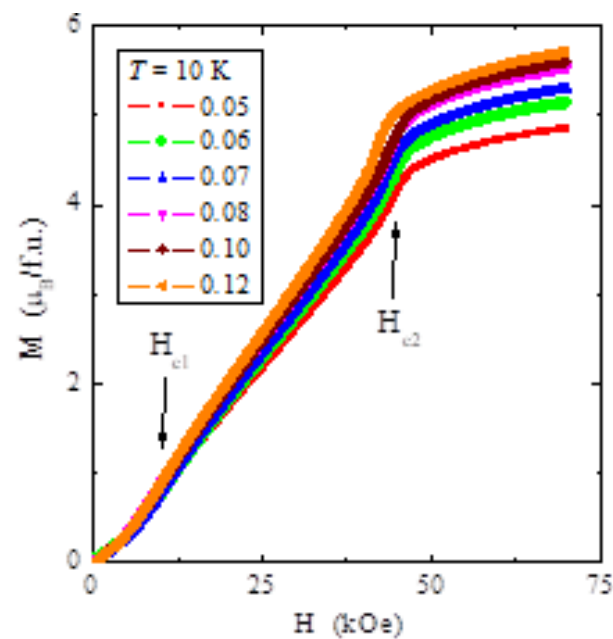


**Figure 8.** Magnetisation  $M$  vs. temperature  $T$  of  $\text{ZnCr}_{2-x}\text{Ta}_x\text{Se}_4$  single crystals (where  $x = 0.05, 0.06, 0.07, 0.08, 0.10$  and  $0.12$ ) recorded at 10 K. Critical fields  $H_{c1}$  and  $H_{c2}$  are indicated by arrows.

**Table 5.** Magnetic parameters of  $\text{ZnCr}_{2-x}\text{Ta}_x\text{Se}_4$  spinels— $C$  is the Curie constant,  $T_N$  is the Néel temperature,  $\theta_{CW}$  is the Curie–Weiss temperature,  $\mu_{eff}$  is the effective magnetic moment,  $p_{eff}$  is the effective number of Bohr magnetons,  $J_1$  and  $J_2$  are the superexchange integrals for the first two coordination spheres,  $H_{c1}$  and  $H_{c2}$  are the critical fields. Experimental data for  $\text{ZnCr}_2\text{Se}_4$  were taken from Ref. [30] for comparison.

Spinel	$C$ (emu $\times$ K/mol)	$T_N$ (K)	$\theta_{CW}$ (K)	$\mu_{eff}$ ( $\mu_B/f.u.$ )	$M_{(10K)}$ ( $\mu_B/f.u.$ )	$P_{eff}$	$J_1$ (K)	$J_2$ (K)	$H_{c1}$ (kOe)	$H_{c2}$ (kOe)
$\text{ZnCr}_2\text{Se}_4$	4.08	21	90	5.71	6.0	5.477	−1.65	1.28	10.0	65.0
$\text{ZnCr}_{1.95}\text{Ta}_{0.05}\text{Se}_4$	4.563	22.7	50.3	6.041	4.85	5.408	−2.57	0.99	10.0	43.5
$\text{ZnCr}_{1.94}\text{Ta}_{0.06}\text{Se}_4$	4.944	22.6	41.5	6.288	5.13	5.394	−2.70	0.91	10.4	43.9
$\text{ZnCr}_{1.93}\text{Ta}_{0.07}\text{Se}_4$	4.278	22.4	58.8	5.849	5.30	5.381	−2.38	1.05	10.7	42.7
$\text{ZnCr}_{1.92}\text{Ta}_{0.08}\text{Se}_4$	2.971	22.3	96.1	4.875	5.54	5.367	−1.74	1.36	10.7	45.6
$\text{ZnCr}_{1.90}\text{Ta}_{0.10}\text{Se}_4$	3.630	22.5	79.1	5.388	5.61	5.339	−2.06	1.22	10.2	43.3
$\text{ZnCr}_{1.88}\text{Ta}_{0.12}\text{Se}_4$	3.696	21.9	78.4	5.437	5.71	5.310	−1.98	1.20	10.4	42.2

The magnetisation isotherms depicted in Figure 7 at 10, 20, 30, 40 and 60 K show characteristic behaviour for the AFM order of magnetic moments and a lack of saturation in the magnetic field of 70 kOe, below the Néel temperature. Magnetisation isotherms plotted at 10 K for all samples show two critical fields and an unexpected increase in the magnetic moment with the rise in the tantalum content (Figure 8). Arrows indicate the metamagnetic transition at the first critical field  $H_{c1}$ , and the breakdown of the helical spin arrangement at the second critical field  $H_{c2}$  in Figure 8. The values of both critical fields weakly depend on the tantalum content in the sample. However, the tantalum ions strongly reduce the second critical field by approximately 20 kOe to that for the  $\text{ZnCr}_2\text{Se}_4$  matrix [30], without significantly affecting the content of the first critical field. The result is a lack of magnetisation saturation above the second critical field due to weaker short-range ferromagnetic interactions.

### 3.4. Heat Capacity

Figures 9 and 10 show the change in the temperature  $T_N$  with the increasing magnetic field  $B$ .

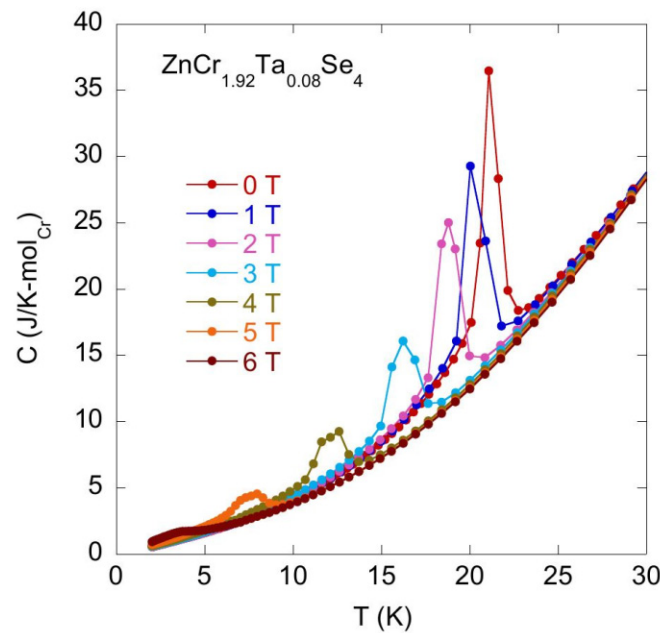


**Figure 9.** Specific heat  $C$  vs. temperature  $T$  measured for  $\text{ZnCr}_{1.92}\text{Ta}_{0.08}\text{Se}_4$  at zero and external magnetic fields.

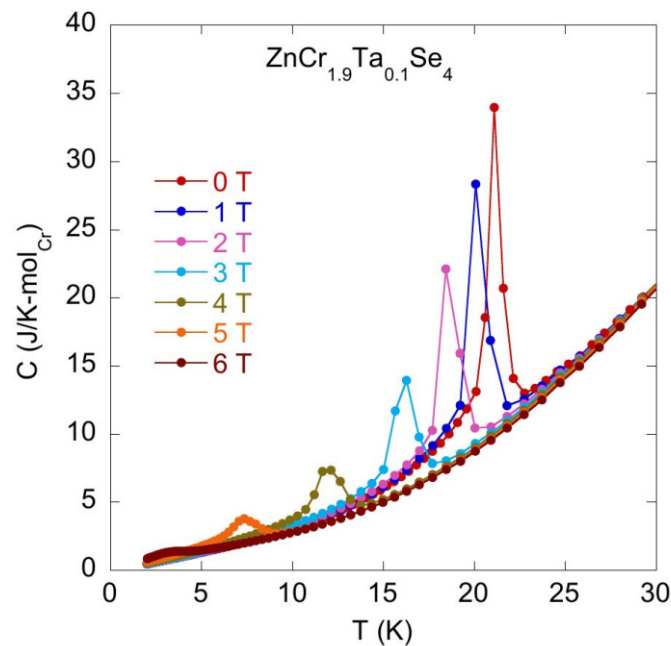


**Figure 10.** Specific heat  $C$  vs. temperature  $T$  measured for  $\text{ZnCr}_{1.90}\text{Ta}_{0.10}\text{Se}_4$  at zero and external magnetic fields.

The specific heat experimental data obtained for the series of various  $\text{Zn}_1\text{Cr}_{2-x}\text{Ta}_x\text{Se}_4$  ( $x = 0.05 - 0.12$ ) compounds show very similar behaviour in the  $C_B(T)$  characteristics obtained at different magnetic fields, which suggests that either the off-stoichiometry in Zn and/or Cr sites or Ta doping do not change the magnetic properties of the pristine  $\text{ZnCr}_2\text{Se}_4$  compound. The magnetic field strongly decreases the temperature  $T_N$  characteristic of the magnetic transitions and decreases the intensity of the  $C$  peak at  $T_N$ . Figure 11 plots  $[T_N(B) - T_N(B = 0)]/T_N(0)$  versus magnetic field  $B$ . It should be noted that  $[T_N(B) - T_N(B = 0)]/T_N(0) \sim B^2$ , which is characteristic behaviour of the antiferromagnetic materials.

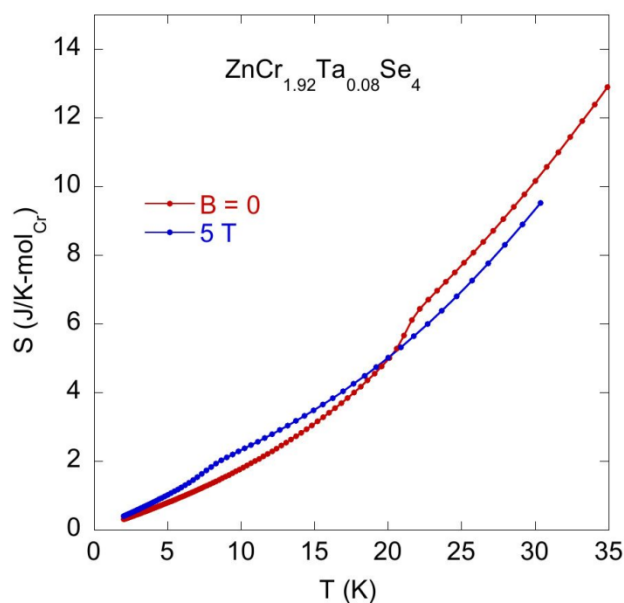


**Figure 11.** Entropy  $S$  per one Cr ion vs. temperature at the magnetic fields  $B = 0$  and 5 T obtained for  $\text{ZnCr}_{1.92}\text{Ta}_{0.08}\text{Se}_4$ .

Figure 12 displays entropy  $S(T) = \int_0^T \frac{C(T)}{T} dT$  calculated at the magnetic fields  $B = 0$  and 5 T, respectively. For all investigated samples, the value of the magnetic and phonon contribution to the entropy at the ordering temperature  $T_N$  and  $B = 0$  is around 50% of the entropy expected, considering the magnetic contribution  $S_m = R \times \ln(2S + 1) = 11.52 \text{ J/Kmol}_{\text{Cr}}$ . The field dependence of  $C$  shown in Figure 12 is associated with the metamagnetic transition at the first critical field  $H_{c1}$ . A very similar  $C_B(T)$  behaviour was experimentally documented recently for a series of spinels, which did not show a change in the magnetic structure at  $H_{c2}$ . Figure 12 also indicates magnetic contribution  $\Delta S(T) = S(T, B = 0) - S(T, B = 5 \text{ T})$  for temperatures  $T > T_N$ , which seems to be characteristic of the family of doped  $\text{ZnCr}_2\text{Se}_4$  and recently was discussed as an effect of spin fluctuations in the paramagnetic regime [14].

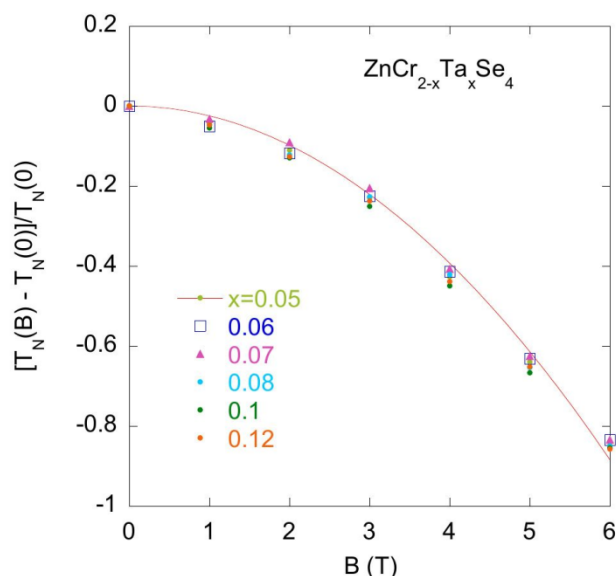


**Figure 12.** The expression  $[T_N(B) - T_N(B = 0)]/T_N(0)$  vs. magnetic field for the series of  $\text{ZnCr}_{2-x}\text{Ta}_x\text{Se}_4$  samples ( $x = 0.05, 0.06, 0.07, 0.08, 0.1$  and  $0.12$ ). The  $[T_N(B) - T_N(B = 0)]/T_N(0)$  data are well approximated by the function  $f(B) = -aB^2$ .

### 3.5. Thermal Analysis

For the thermal measurements, the single crystals with a more significant amount of Ta were chosen to show the changes in thermal properties under the influence of Ta. The thermogravimetric (TG) results and differential scanning calorimetry (DSC) measurements vs. temperature are shown in Figure 13 for the  $\text{ZnCr}_{1.90}\text{Ta}_{0.10}\text{Se}_4$  single crystals.

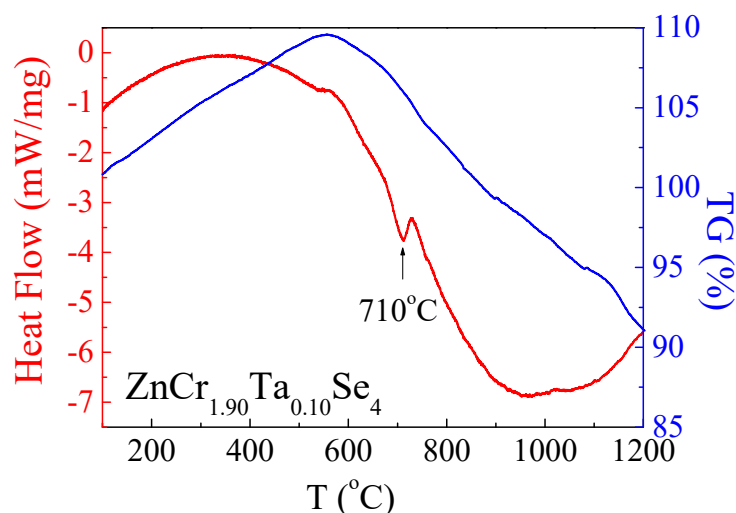


Figure 13. DSC/TG curves for  $\text{ZnCr}_{1.90}\text{Ta}_{0.10}\text{Se}_4$  single crystals.

The TG curve shows a mass loss of 34%. This is a similar value to the pure  $\text{ZnCr}_2\text{Se}_4$  (Table 6). The differential scanning calorimetry (DSC) curve showed a small endothermic peak at 710 °C for  $\text{ZnCr}_{1.90}\text{Ta}_{0.10}\text{Se}_4$ , which confirmed that the melting effect occurs at a high temperature. These peaks indicate that, for the investigated crystals, the melting effect appears at high temperatures. However, a shift in the peak towards lower temperatures was observed. This was caused by additional cations ( $\text{Ta}^{3+}$ ), which caused stiffening of the crystal lattice. On the one hand, this effect could be caused by an increase in covalent binding. On the other hand, the presence of  $\text{Ta}^{3+}$  ions is a kind of “impurity”, which induces a change in the endothermic peak position. Similar behaviour was observed in the  $(\text{Zn}_{1-x}\text{Nd}_x)\text{Cr}_2\text{Se}_4$  system [20].

Table 6. Parameters determined from TG and DSC analysis for  $\text{ZnCr}_{1.90}\text{Ta}_{0.10}\text{Se}_4$  single crystals. Data for pure  $\text{ZnCr}_2\text{Se}_4$ , presented in [20], are shown for comparison.

Ta Content	Weight Loss (%)	Onset (°)	Endset (°)	Peak Minimum (°)	Peak Height (mW)	Peak Area (J)	Enthalpy (J/g)
0.0	35	735	771	755	6.47	1.09	51.9
0.10	34	693	725	710	4.42	1.83	117.3

## 4. Conclusions

In summary, we have presented new  $\text{ZnCr}_2\text{Se}_4$  single crystals doped with tantalum. The single crystals  $\text{ZnCr}_{2-x}\text{Ta}_x\text{Se}_4$  (where  $x = 0.05, 0.06, 0.07, 0.08, 0.10$  and  $0.12$ ) were obtained by chemical vapour transport (CVT method), examined and analysed with XRD, SEM, DSC/TG, SQUID and QD-PPMS. Structural, electrical, magnetic, specific heat and thermal measurements showed the spinel structure with the presence of tantalum ions as  $\text{Ta}^{3+}$  in the octahedral sites, semiconducting properties in the intrinsic region, AFM order below the Néel temperature of 22 K with the FM short-range interactions as well as a strong shift in the specific heat peak towards lower temperatures with an increase in the magnetic field and a weaker than expected magnetic and phonon contribution to entropy. Generally,

the shift in the specific heat peak and the Néel temperature towards lower temperatures with increasing dc magnetic field is usually accompanied by a phase transition from a cubic to a tetragonal structure. In other words, a strong dc magnetic field broadens the temperature range of the paramagnetic state and the cubic structure of the spinel under study. The upper critical field indicates that the sample reached the state of FM order below the structural transition. The situation is similar in the case of the  $\text{ZnCr}_2\text{Se}_4$  matrix. The greatest influence of tantalum was observed in the increase in magnetisation and reduction in the second critical field.

**Author Contributions:** Conceptualisation, I.J. and T.G. (Tadeusz Groń); methodology, I.J., T.G. (Tadeusz Groń), B.S., and H.D.; validation, I.J.; formal analysis, A.Ś., M.F. and T.G. (Tadeusz Groń); investigation, I.J., P.K., J.K., E.P., T.G. (Tomasz Goryczka), B.S., J.J. and H.D.; resources, I.J.; writing—original draft preparation, I.J., T.G. (Tadeusz Groń) and A.Ś.; writing—review and editing, I.J., T.G. (Tadeusz Groń) and A.Ś.; visualisation, I.J. and T.G. (Tadeusz Groń); supervision, I.J.; project administration, I.J. All authors have read and agreed to the published version of the manuscript.

**Funding:** The research is a part of National Science Centre of Poland, grant no. N204 151940. This study was partially supported by the Slovak Research and Development Agency (APVV-17-0318).

**Institutional Review Board Statement:** Not applicable.

**Informed Consent Statement:** Not applicable.

**Data Availability Statement:** The data presented in this study are available on request from the corresponding author.

**Conflicts of Interest:** The authors declare no conflict of interest.

## References

1. Snyder, G.J.; Caillat, T.; Fleurial, J.P. Thermoelectric properties of Chalcogenides with Spinel Structure. *Mat. Res. Innov.* **2001**, *5*, 67. [[CrossRef](#)]
2. Groń, T.; Malicka, E.; Pacyna, A.W. Influence of temperature on critical fields in  $\text{ZnCr}_2\text{Se}_4$ . *Physica B* **2009**, *404*, 3554–3558. [[CrossRef](#)]
3. Malicka, E.; Groń, T.; Ślebarski, A.; Pacyna, A.W.; Goraus, J.; Fijałkowski, M.; Heimann, J. Specific heat and magnetic susceptibility of single-crystalline  $\text{ZnCr}_{2-x}\text{Al}_x\text{Se}_4$  ( $x = 0.15, 0.23$ ). *J. Phys. Chem. Solids* **2011**, *72*, 974–979. [[CrossRef](#)]
4. Malicka, E.; Groń, T.; Pacyna, A.W.; Gaĝor, A.; Mydlarz, T. Spin-driven critical fields in a spinel series based on the matrix  $\text{ZnCr}_2\text{Se}_4$ . *J. Phys. Conf. Ser.* **2011**, *303*, 012077. [[CrossRef](#)]
5. Malicka, E.; Groń, T.; Ślebarski, A.; Gaĝor, A.; Pacyna, A.W.; Sitko, R.; Goraus, J.; Mydlarz, T.; Heimann, J. Specific heat and magnetic susceptibility of single-crystalline  $\text{ZnCr}_2\text{Se}_4$  spinels doped with Ga, In and Ce. *Mater. Chem. Phys.* **2011**, *131*, 142–150. [[CrossRef](#)]
6. Akimitsu, J.; Siraatori, K.; Shirane, G.; Iizumi, M.; Watanabe, T. Neutron Scattering Study of  $\text{ZnCr}_2\text{Se}_4$  with Screw Spin Structure. *J. Phys. Soc. Jpn.* **1978**, *44*, 172–180. [[CrossRef](#)]
7. Suga, S.; Shin, S.; Taniguchi, M.; Inoue, K.; Seki, M.; Nakada, I.; Shibuya, S.; Yamaguchi, T. Reflectance spectra of  $\text{ZnCr}_2\text{Se}_4$  spinel from 4 to 100 eV measured with synchrotron radiation: Band structure, covalency, and final-state interactions. *Phys. Rev. B* **1982**, *25*, 5486. [[CrossRef](#)]
8. Yaresko, A.N. Electronic band structure and exchange coupling constants in  $\text{ACr}_2\text{X}_4$  spinels ( $A = \text{Zn, Cd, Hg}$ ;  $X = \text{O, S, Se}$ ). *Phys. Rev. B* **2008**, *77*, 115106. [[CrossRef](#)]
9. Rudolf, T.; Kant, C.; Mayr, F.; Schmidt, M.; Tsurkan, V.; Deisenhofer, J.; Loidl, A. Optical properties of  $\text{ZnCr}_2\text{Se}_4$ . *Eur. Phys. J. B* **2009**, *68*, 153–160. [[CrossRef](#)]
10. Plumier, R. Étude par diffraction de neutrons de l'antiferromagnétisme hélicoïdal du spinelle  $\text{ZnCr}_2\text{Se}_4$  en présence d'un champ magnétique. *J. Phys.* **1966**, *27*, 213–219. [[CrossRef](#)]
11. Cameron, A.S.; Tymoshenko, Y.V.; Portnichenko, P.Y.; Gavilano, J.; Tsurkan, V.; Felea, V.; Loidl, A.; Zherlitsyn, S.; Wosnitza, J.; Inosov, D.S. Magnetic phase diagram of the helimagnetic spinel compound  $\text{ZnCr}_2\text{Se}_4$  revisited by small-angle neutron scattering. *J. Phys. Condens. Matter* **2016**, *28*, 146001. [[CrossRef](#)]
12. Groń, T. Influence of vacancies and mixed valence on the transport processes in solid solutions with the spinel structure. *Philos. Mag. B* **1994**, *70*, 121–132. [[CrossRef](#)]
13. Jendrzejewska, I.; Groń, T.; Kusz, J.; Żelechower, M.; Maciążek, E.; Ślebarski, A.; Fijałkowski, M. Spin-glass-like behaviour in tin doped  $\text{ZnCr}_2\text{Se}_4$  single crystals. *J. Alloys Compd.* **2015**, *635*, 238–244. [[CrossRef](#)]
14. Maciążek, E.; Karolus, M.; Kubisztal, M.; Jendrzejewska, I.; Sitko, R.; Groń, T.; Ślebarski, A.; Fijałkowski, M. Magnetic and specific heat properties of a new Gd-doped  $\text{ZnCr}_2\text{Se}_4$ . *Mater. Chem. Phys.* **2015**, *168*, 187–192. [[CrossRef](#)]

15. Jendrzewska, I.; Groń, T.; Knizek, K.; Pilch, M.; Ślebarski, A.; Goraus, J.; Zajdel, P.; Stokłosa, Z.; Pietrasik, E.; Goryczka, T.; et al. Preparation, structure and magnetic, electronic and thermal properties of Dy<sup>3+</sup>-doped ZnCr<sub>2</sub>Se<sub>4</sub> with unique geometric type spin-glass. *J. Sol. State Chem.* **2021**, *298*, 122114. [[CrossRef](#)]
16. Duda, H.; Groń, T.; Jendrzewska, I.; Mazur, S.; Zajdel, P.; Kita, A. Polaron conductivity of the strongly defective ZnCr<sub>2-x</sub>Ni<sub>x</sub>Se<sub>4</sub> spinels. *Phys. Stat. Sol.* **2007**, *4*, 1309–1312. [[CrossRef](#)]
17. Jendrzewska, I.; Mydlarz, T.; Okońska-Kozłowska, I.; Heimann, J. Magnetic properties of single crystals Cu<sub>x</sub>Zn<sub>y</sub>Cr<sub>z</sub>Se<sub>4</sub>. *J. Magn. Mater.* **1998**, *186*, 381–385. [[CrossRef](#)]
18. Jendrzewska, I.; Groń, T.; Goraus, J.; Pilch, M.; Pietrasik, E.; Barsova, Z.; Czerniewski, J.; Goryczka, T.; Witkowska-Kita, B.; Bienko, A.; et al. Synthesis and structural, magnetic, thermal and electronic properties of Mn-doped ZnCr<sub>2</sub>Se<sub>4</sub>. *Mater. Chem. Phys.* **2019**, *238*, 121901. [[CrossRef](#)]
19. Jendrzewska, I.; Zajdel, P.; Heimann, J.; Krok-Kowalski, J.; Mydlarz, T.; Mrzigod, J. Influence of manganese on magnetic and electronic properties of ZnCr<sub>2</sub>Se<sub>4</sub> single Crystals. *Mater. Res. Bull.* **2012**, *47*, 1881–1886. [[CrossRef](#)]
20. Jendrzewska, I.; Groń, T.; Kusz, J.; Barsova, Z.; Pietrasik, E.; Goryczka, T.; Sawicki, B.; Ślebarski, A.; Fijałkowski, M.; Jampilek, J.; et al. Synthesis, crystal structure and characterization of monocrystalline ZnCr<sub>2</sub>Se<sub>4</sub> doped with neodymium. *J. Sol. State Chem.* **2020**, *292*, 121661. [[CrossRef](#)]
21. Jendrzewska, I.; Groń, T.; Kusz, J.; Goraus, J.; Barsova, Z.; Pietrasik, E.; Czerniewski, J.; Goryczka, T.; Kubisztal, M. Growth, structure and physico-chemical properties of monocrystalline ZnCr<sub>2</sub>Se<sub>4</sub>:Ho prepared by chemical vapour transport. *J. Sol. State Chem.* **2020**, *281*, 121024. [[CrossRef](#)]
22. Jendrzewska, I.; Żelechower, M.; Szamocka, K.; Mydlarz, T.; Waśkowska, A.; Okońska-Kozłowska, I. Growth of the Cd<sub>x</sub>Ni<sub>y</sub>Cr<sub>z</sub>Se<sub>4</sub> single crystals and their magnetic properties. *J. Cryst. Growth* **2004**, *270*, 30–37. [[CrossRef](#)]
23. Sheldrick, G.M. A short history of SHELX. *Acta Crystallogr. C* **2015**, *71*, 3–8. [[CrossRef](#)] [[PubMed](#)]
24. Groń, T.; Krok-Kowalski, J.; Duda, H.; Mydlarz, T.; Gilewski, A.; Walczak, J.; Filipek, E.; Bärner, K. Metamagnetism in the Cr<sub>2</sub>V<sub>4-x</sub>Mo<sub>x</sub>O<sub>13+0.5x</sub> solid solutions. *Phys. Rev. B* **1995**, *51*, 16021–16024. [[CrossRef](#)] [[PubMed](#)]
25. Groń, T.; Krok-Kowalski, J.; Pacyna, A.W.; Mydlarz, T. Spin-glass-like behaviour and magnetic order in Mn[Cr<sub>0.5</sub>Ga<sub>1.5</sub>]S<sub>4</sub> spinels. *J. Phys. Chem. Sol.* **2009**, *70*, 900–905. [[CrossRef](#)]
26. Holland, W.E.; Brown, H.A. Application of the Weiss molecular field theory to the B-site spinel. *Phys. Status Sol. A* **1972**, *10*, 249–253. [[CrossRef](#)]
27. Shannon, R.D. Revised Effective Ionic Radii and Systematic Studies of Interatomic Distances in Halides and Chalcogenides. *Acta Crystallogr. A* **1976**, *32*, 751–767. [[CrossRef](#)]
28. Malicka, E.; Groń, T.; Skrzypek, D.; Pacyna, A.W.; Badurski, D.; Waśkowska, A.; Mazur, S.; Sitko, R. Correlation between the negative magnetoresistance effect and magnon excitations in single-crystalline CuCr<sub>1.6</sub>V<sub>0.4</sub>Se<sub>4</sub>. *Philos. Mag.* **2010**, *90*, 1525–1541. [[CrossRef](#)]
29. Watanabe, T. Electrical Resistivity and Hall Effect of ZnCr<sub>2</sub>Se<sub>4</sub>. *J. Phys. Soc. Jpn.* **1974**, *37*, 140–144. [[CrossRef](#)]
30. Hemberger, J.; von Nidda, H.-A.K.; Tsurkan, V.; Loidl, A. Large Magnetostriction and Negative Thermal Expansion in the Frustrated Antiferromagnet ZnCr<sub>2</sub>Se<sub>4</sub>. *Phys. Rev. Lett.* **2007**, *98*, 147203. [[CrossRef](#)]